Available online at www.sciencedirect.com

ScienceDirect

www.elsevier.com/locate/jes

JES JOURNAL OF ENVIRONMENTAL SCIENCES

www.jesc.ac.cn

Fabrication of electrochemically-modified $BiVO_4$-MoS_2-Co_3O_4composite film for bisphenol A degradation

Yanqing Cong[1,2], *Wenhua Zhang*[1], *Wenchen Ding*[1], *Tongtong Zhang*[1], *Yi Zhang*[1,2], *Nianping Chi*[1], *Qi Wang*[1,2,*]

[1] *School of Environmental Science and Engineering, Zhejiang Gongshang University, Hangzhou 310018, China*
[2] *Institute of Urban Aquatic Environment, Zhejiang Gongshang University, Hangzhou 310018, China*

ARTICLE INFO

Article history:
Received 28 July 2020
Revised 23 September 2020
Accepted 24 September 2020
Available online 20 October 2020

Keywords:
Electrochemically-modified $BiVO_4$-MoS_2-Co_3O_4
Photoelectrocatalytic (PEC)
Electrochemical modification
Visible light
Bisphenol A (BPA)

ABSTRACT

A new electrochemically-modified $BiVO_4$-MoS_2-Co_3O_4 (represented as E-$BiVO_4$-MoS_2-Co_3O_4) thin film electrode was successfully synthesized for environmental application. MoS_2 and Co_3O_4 were grown on the surface of $BiVO_4$ to obtain $BiVO_4$-MoS_2-Co_3O_4. E-$BiVO_4$-MoS_2-Co_3O_4 film was achieved by further electrochemical treatment of $BiVO_4$-MoS_2-Co_3O_4. The as-prepared E-$BiVO_4$-MoS_2-Co_3O_4 exhibited significantly enhanced photoelectrocatalytic activity. The photocurrent density of E-$BiVO_4$-MoS_2-Co_3O_4 thin film is 6.6 times that of $BiVO_4$ under visible light irradiation. The degradation efficiency of E-$BiVO_4$-MoS_2-Co_3O_4 for bisphenol A pollutant was 81.56% in photoelectrochemical process. The pseudo-first order reaction rate constant of E-$BiVO_4$-MoS_2-Co_3O_4 film is 3.22 times higher than that of $BiVO_4$. And its reaction rate constant in photoelectrocatalytic process is 14.5 times or 2 times that in photocatalytic or electrocatalytic process, respectively. The improved performance of E-$BiVO_4$-MoS_2-Co_3O_4 was attributed to the synergetic effects of the reduction of interfacial charge transfer resistance, the formation of oxygen vacancies and sub-stoichiometric metal oxides and higher separation efficiency of photogenerated electron-hole pairs. E-$BiVO_4$-MoS_2-Co_3O_4 is a promising composite material for pollutants removal.

Introduction

Environmental and resource issues are attracting more and more attentions due to environmental pollution and resource shortage. Emerging contaminants (ECs) such as medicines, cosmetics, endocrine disrupting chemicals, polycyclic aromatic hydrocarbons (PAHs), and so on have potential threats to the environment and human health even at low concentration due to their stable chemical properties and easy bioaccumulation (Giulivo et al., 2016; Zia et al., 2019; Liu and Zhao, 2020). For example, endocrine disrupting chemicals (EDCs) can cause endocrine imbalances and result in reduced fertility, carcinogenicity and teratogenesis, neurotoxicity and immune diseases (Bui et al., 2016; Wu et al., 2020). Therefore, it is urgent to develop an environment-friendly technology to remove these contaminants.

Solar energy and electric energy, as clean energy, are considered as the most promising energy in the future

* Corresponding author
E-mail: wangqi8327@mail.zjgsu.edu.cn (Q. Wang).

https://doi.org/10.1016/j.jes.2020.09.027
1001-0742/

(Fujishima and Honda, 1972; Zhang et al., 2018a). As a green and efficient advanced oxidation process, the photoelectrocatalytic (PEC) technology has attracted much attention because of its excellent performance in rapidly and thoroughly oxidizing organic pollutants (Zhang et al., 2017a). In PEC process, a bias potential is applied to further promote the separation of photogenerated electron-hole pairs of semiconductor electrode, which was confirmed to be superior to single photocatalytic process (Wang et al., 2012, 2015; Cong et al., 2016; Regmi et al., 2019). In addition, the film catalyst fixed on the conductive electrode in PEC process is easier to reuse than the powder catalyst, and can avoid secondary pollution problems. Many semiconductor materials with visible light response have been developed to degrade the contaminants (Guo et al., 2016; Huang et al., 2017; Gauvin et al., 2018; Malathi et al., 2018; Zhang et al., 2018b). Bismuth-based materials, such as BiOX (X = Cl, Br, I), Bi_2WO_6, $Bi_2O_2CO_3$ and $BiVO_4$, have attracted researchers' attentions due to their unique physical properties under visible light irradiation (Chen et al., 2016; Hu et al., 2018; Sun et al., 2019). Among them, $BiVO_4$ is considered to be a good photocatalytic material due to its narrow band gap (2.4 eV) and wide visible wavelength range (Zhu et al., 2018; Regmi et al., 2019). However, the high recombination of photo-induced electrons and holes is an obstacle to the realization of efficient photocatalytic performance. It is an efficient method that coupling two or more semiconductors reduces the recombination of photo-generated electron-hole pairs (Chen et al., 2017).

Molybdenum disulfide (MoS_2), as a special layered material, is widely used in various fields due to its small band gap, excellent electron accepting and transporting performance and good stability (Yu et al., 2016). The construction of $BiVO_4/MoS_2$ composites could improve the PEC performance of $BiVO_4$ since the band gap position of MoS_2 match with $BiVO_4$ (Arora et al., 2016; Pan et al., 2018). However, the activity of binary $BiVO_4/MoS_2$ composites is still very low in practical applications. As an important co-catalyst, Co_3O_4 has the advantages of low cost, good activity and stability, which could significantly improve the photocatalytic activity of the composite materials (Bao et al., 2016; Liu et al., 2011; Mo et al., 2019). Previous studies have shown that the binary heterojunction constructed by adding Co_3O_4 to $BiVO_4$ can greatly improve the catalytic performance of $BiVO_4$ (Wang and Osterloh, 2014; Li et al., 2019) Therefore, Co_3O_4 is selected to fabricate a ternary structure with $BiVO_4/MoS_2$ to further improve its performance.

In addition, forming sub-stoichiometric metal oxides was confirmed to be more efficient to increase the carrier densities and improve the PEC performance of metal oxides (Wang et al., 2016). Hydrogenation can achieve the sub-stoichiometry by reducing the metal oxides in hydrogen gas at high temperature (Chen et al., 2011; Harthcock et al., 2020). However, high-temperature hydrogenation is energy-intensive and has potential safety risk. Electrochemical modification has been proved to be an effective strategy for obtaining the sub-stoichiometry in the original metal oxide at normal temperatures and pressures (Wang et al., 2017; Cong et al., 2020). It is convenient to control the quantity of sub-stoichiometric metal oxides by adjusting the treatment time and potential in electrochemical modification. Therefore, the preparation of $BiVO_4$-MoS_2-Co_3O_4 thin films modified by electrochemical treatment (represented as E-$BiVO_4$-MoS_2-Co_3O_4) was expected to achieve perfect PEC performance. As far as we know, E-$BiVO_4$-MoS_2-Co_3O_4 has not been reported.

In this study, $BiVO_4$-MoS_2-Co_3O_4 thin film electrode was synthesized by hydrothermal, electrodeposition and calcination methods, and its photocatalytic activity was further improved by electrochemical modification. X-ray diffraction (XRD), X-ray photoelectron spectroscopy (XPS) and scanning electron microscope (SEM) were used to characterize the as-prepared films. PEC properties of E-$BiVO_4$-MoS_2-Co_3O_4 in visible light were studied by linear sweep voltammetry (LSV), Nyquist spectrum and incident monochromatic photon-current conversion efficiency (IPCE). Bisphenol A (BPA) is one of emerging contaminants, which can cause endocrine disorders, and threaten the health of the fetus and children. In addition, cancer and obesity caused by metabolic disorders are also thought to be related to BPA contamination (Liu and Zhao, 2020). Therefore, BPA was selected as colorless model pollutant to study the performance of E-$BiVO_4$-MoS_2-Co_3O_4 in removing refractory pollutants. The effects of photocatalysis (PC), electrocatalysis (EC) and PEC were studied. The degradation experiments were carried out to study the reaction mechanism.

1. Materials and methods

1.1. Chemicals

Bismuth nitrate pentahydrate ($Bi(NO_3)_3{\cdot}5H_2O$), ethylene glycol, formamide, acetone, and boric acid (H_3BO_3) were all obtained from Chengdu Kelong Chemical Reagent Co., Ltd. (Sichuan, China). Diammoniumthiomolybdate ($(NH_4)_2MoS_4$) was got from Beijing Bailingwei Technology Co., Ltd. (Beijing China). Polyvinyl alcohol (PVA), ammonium metavanadate (NH_4VO_3), and cobalt nitrate hexahydrate ($Co(NO_3)_2{\cdot}6H_2O$) were purchased from Shanghai Macklin Biochemical Co., Ltd. (Shanghai, China). All reagents were used as received without further purification.

1.2. Synthesis of E-$BiVO_4$-MoS_2-Co_3O_4 films

Fluorine-doped tin oxide substrate (FTO, Nippon Sheet Glass Co Ltd) is used as a substrate material for electrode preparation. The FTO (10 mm × 50 mm × 2.2 mm) was ultrasonically cleaned with acetone, ethanol and deionized water for 10 min to remove the impurities on the surface, and then dried in air at room temperature for use. The preparation processes of $BiVO_4$, $BiVO_4$-MoS_2, $BiVO_4$-MoS_2-Co_3O_4 and E-$BiVO_4$-MoS_2-Co_3O_4 films were shown in Appendix A **Fig. S1**.

(1) Preparation of $BiVO_4$ film: 0.1164 g of $Bi(NO_3)_3{\cdot}5H_2O$ and 0.028 g of NH_4VO_3 were dissolved in 60 mL of distilled water containing 1.6 mL of concentrated HNO_3 (70 wt.%). Subsequently, 15 mL solution was transferred to a 50 mL Teflon-lined stainless steel autoclave, and the FTO substrate was immersed in the solution for hydrothermal reaction at 180°C for 12 hr. The resulting film was rinsed with

deionized water and finally calcined at 450°C for 2 hr in an air atmosphere to obtain a stable $BiVO_4$ thin film electrode.

(2) Preparation of $BiVO_4$-MoS_2 film: 0.026 g of diammoniumthiomolybdate ($(NH_4)_2MoS_4$), 0.149 g of potassium chloride (KCl) and 0.535 g of ammonium chloride (NH_4Cl) were dissolved in 50 mL of formamide to prepare an electrodeposition solution. Electrodeposition was carried out in a three-electrode system using CHI 660E electrochemical workstation (Chenhua, Shanghai). The $BiVO_4$ film was used as the working electrode. The titanium plate and the saturated Ag/AgCl were used as the counter electrode and reference electrode, respectively. The electrodeposition was performed at the voltage of −0.6 V for 15 min to obtain a $BiVO_4$-MoS_2 photocatalytic film.

(3) Preparation of $BiVO_4$-MoS_2-Co_3O_4 film: The $BiVO_4$-MoS_2 film was immersed in a 0.03 mol/L cobalt nitrate solution for 30 min and then taken out to anneal at 400°C for 1 hr under N_2 atmosphere to obtain the $BiVO_4$-MoS_2-Co_3O_4 photocatalytic film.

(4) Preparation of E-$BiVO_4$-MoS_2-Co_3O_4 film: According to the previous work of our group (Cong et al., 2020), electrochemical modification was carried out using a three-electrode system by a CHI 660E electrochemical workstation. The $BiVO_4$-MoS_2-Co_3O_4 film was used as the working electrode. The platinum plate and Ag/AgCl electrode were used as the counter electrode and the reference electrode, respectively. The electrolyte was 1 mol/L boric acid solution and pH was adjusted to ~9.5 using potassium hydroxide. The film was treated at a voltage of −0.8 V for 150 sec to obtain an E-$BiVO_4$-MoS_2-Co_3O_4 photocatalytic film.

1.3. Characterization

X-ray diffraction (XRD) patterns were collected on a Bruker D8 advance powder diffract meter (D8 advance, Bruker AXS, Germany) at Cu-$K\alpha$ (Test wavelength $\lambda = 0.154056$ nm) in the 2θ range of 10–70°. X-ray photoelectron spectroscopy (XPS, Thermo ESCALAB 250Xi spectrometer with Al-$K\alpha$ at 1486.6 eV) was used to analyze the chemical composition and surface chemical state of the prepared samples (XLESCALAB 250Xi, Thermo fisher scientific, USA). The binding energy is corrected by C 1 s (284.6 eV). Scanning electron microscopy (SEM, Gemini SEM 500, ZEISS, Germany) was used to characterize the morphology, particle size and structure of the prepared catalytic films.

1.4. PEC measurements

PEC performance of the as-prepared film electrodes were all tested in the three-electrode system using CHI 660E electrochemical workstation. A xenon lamp with a UV 420 nm cutoff filter was used as an illumination source and the incident light intensity was ~100 mW/cm^2. The platinum plate and Ag/AgCl electrode were used as the counter electrode and the reference electrode, respectively. The working electrode was the as-prepared thin film. Linear sweep voltammetry (LSV) was used to investigate the photocurrent densities of as-prepared photoelectrodes in 0.1 mol/L NaOH solution under dark/light conditions. Electrochemical impedance spectroscopy (EIS) was performed with an amplitude of 5 mV and a frequency of 0.01–10^5 Hz at 0 V vs. Ag/AgCl. The monochromatic incident photon-to-electron conversion efficiency (IPCE) was measured in 0.1 mol/L Na_2SO_4 and 0.1 mol/L Na_2SO_3 mixed solution at 0.4 V vs. Ag/AgCl by a xenon lamp equipped with different monochromatic filters (400, 430, 475, 500, 550, and 600 nm).

1.5. PEC degradation of BPA

Bisphenol A (BPA) was used as a representative of emerging contaminants to investigate the degradation performance of the as-prepared films. The PEC degradation of BPA (10 mg/L) was carried out in a two-electrode system. The as-prepared film (active area 4 cm^2) was used as the anode, and the titanium plate was used as the cathode. Na_2SO_4 (0.2 mol/L) was used as an electrolyte solution. Before the PEC reaction, the dark reaction was carried out for 30 min to achieve the adsorption-desorption equilibrium between BPA and the photocatalytic film. Then an appropriate voltage and visible light irradiation were applied to initiate the reaction. Similar to the steps of the above photoelectrocatalytic degradation experiment, different scavengers are added to the reaction solution to evaluate related active substances. Benzoquinone (10 mmol/L) is used to remove $O_2^{\cdot-}$, 10 mmol/L oxalic acid is used to capture active hole (h^+), and 10 mmol/L *tert*-butanol is used to remove $HO^{\cdot}$. The concentration of BPA was determined by high-performance liquid chromatography (HPLC, Agilent1200 infinity, Agilent Corporation, USA) with Diamonsil C18 column and wavelength detection at 278 nm. A mixture of methanol and water (60:40) was used as the mobile phase. BPA removal rate (η) was calculated according to formula (1):

$$\eta(\%) = (C_0 - C_t)/C_0 \times 100\% \quad (1)$$

where C_0 (mg/L) and C_t (mg/L) represent the initial BPA concentration and the BPA concentration at reaction time t (min), respectively.

A total organic carbon analyzer (TOC-L CPN, Shimadzu, Japan,) was used to evaluate the mineralization degree. The generation of $O_2^{\cdot-}$ was measured by electron spin resonance (ESR) spectroscopy (ESR A200, Bruker, Germany).

2. Results and discussion

2.1. Characterization

The morphologies of $BiVO_4$, $BiVO_4$-MoS_2, $BiVO_4$-MoS_2-Co_3O_4 and E-$BiVO_4$-MoS_2-Co_3O_4 were analyzed by SEM. As shown in Fig. 1**a**, the $BiVO_4$ is granular with the average width of 480 nm and the spatial structure is relatively tight. For $BiVO_4$-MoS_2, it can be seen from Fig. 1**b** that MoS_2 nanoparticles appear on the surface of $BiVO_4$. The average size of MoS_2 particles is 250 nm long and 150 nm wide. Fig. 1**c** shows the microstructure of $BiVO_4$-MoS_2-Co_3O_4 thin film electrode. More Co_3O_4 nanorods were found on the surface of $BiVO_4$-MoS_2. The length of the nanorod is ~200 nm. After electrochemical modification (Fig. 1**d**), E-$BiVO_4$-MoS_2-Co_3O_4 thin films become more compact, and the connections between the various structures are closer, this could probably facilitate charge transfer. The cross-sectional SEM test of the electrode film is

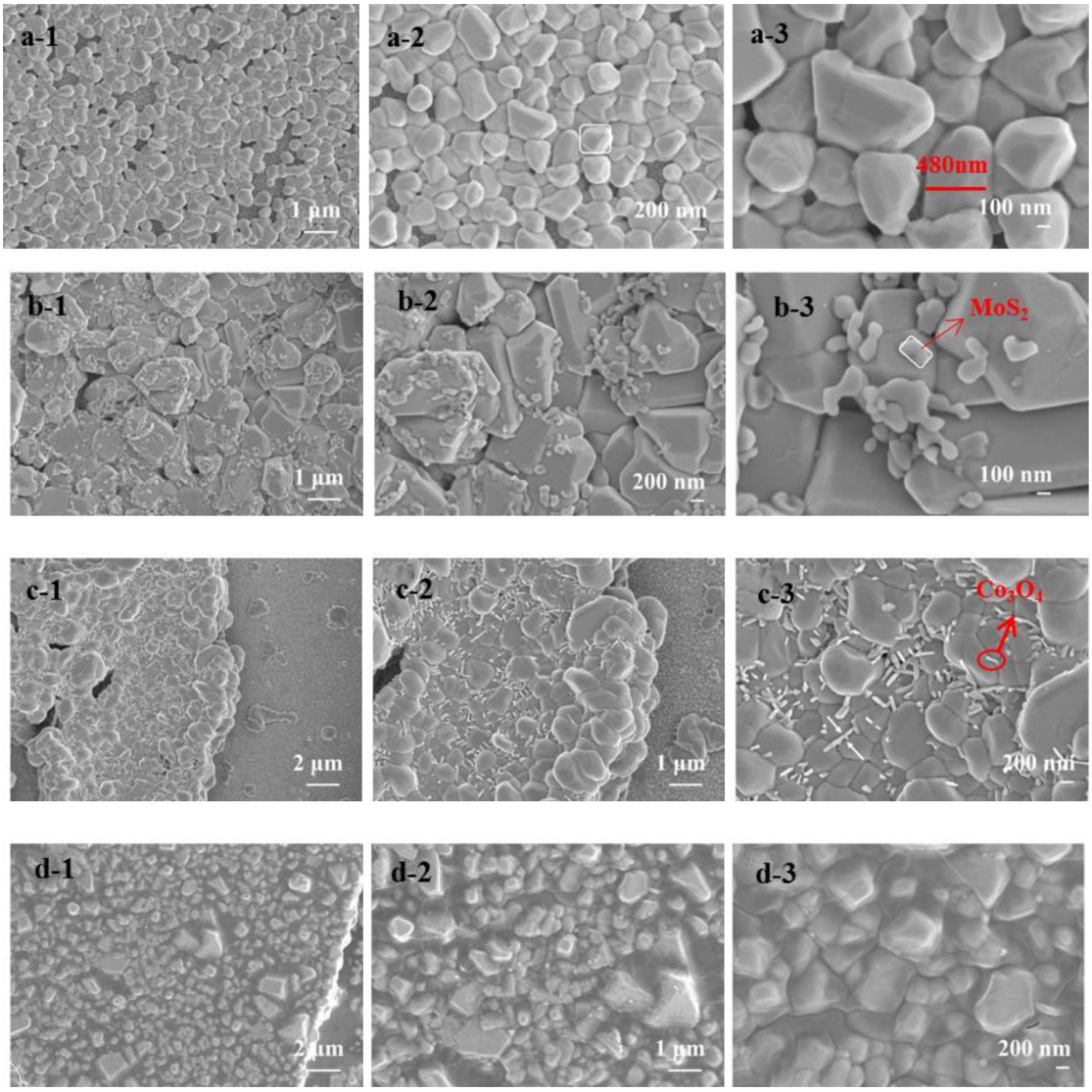

Fig. 1 – Scanning electron microscope (SEM) images of (a) $BiVO_4$, (b) $BiVO_4$-MoS_2, (c) $BiVO_4$-MoS_2-Co_3O_4 and (d) electrochemically-modified $BiVO_4$-MoS_2-Co_3O_4 (E-$BiVO_4$-MoS_2-Co_3O_4) films. The numbers 1, 2, and 3 refer to images with different magnification.

shown in Appendix A **Fig. S2** and it can be seen that the thickness of the E-$BiVO_4$-MoS_2-Co_3O_4 film is 290.3 nm. In addition, the X-ray energy spectrum analysis (EDS) mapping test results (Appendix A **Fig. S3**) show that Co, O, Mo, Bi, S and V are homogeneously distributed over the thin film.

The phase structure and crystal structure of $BiVO_4$, $BiVO_4$-MoS_2, $BiVO_4$-MoS_2-Co_3O_4 and E-$BiVO_4$-MoS_2-Co_3O_4 thin film electrodes were analyzed by X-ray diffraction (XRD). In Fig. 2, the four catalytic materials all have characteristic peaks of $BiVO_4$, and the peaks at 18.7°, 19.1° and 29.0° correspond to the (101), (011) and (112) crystal planes in the $BiVO_4$ standard map (PDF 83–1700) (Su et al., 2011). It indicates that $BiVO_4$ is present in the composite photoelectric film. When MoS_2 was loaded on $BiVO_4$ film, the characteristic diffraction peaks at 15.1°, 34.8°, 39.96° and 58.38° were observed (Fig. 2**b**), which correspond to the (003), (012), (103) and (104) crystal planes in MoS_2 standard map (PDF 17–0744), respectively (Zhang et al., 2014; Sun et al., 2016). When Co_3O_4 was further loaded on $BiVO_4$-MoS_2, two peaks at 36.9° and 59.4° were observed, which correspond to the (311) and (511) crystal planes of Co_3O_4 (PDF 76–1802) (Zhao et al., 2018; Li et al., 2019), respectively. Therefore, MoS_2 and Co_3O_4 are co-loaded on the surface of $BiVO_4$. The enlarged XRD pattern in the range of 28–32° is shown in Appendix A **Fig. S4.** The peak corresponding to 29° in the $BiVO_4$-MoS_2 electrode is weakened compared to that in $BiVO_4$ electrode, while the peak height at ~30.5° is enhanced, and the diffraction peak is obviously shifted to the lower degree. This may be due to the fact that during the preparation of $BiVO_4$-MoS_2, a voltage of −0.6 V was used for electrodeposition, which might cause part of the $BiVO_4$ to be reduced and the peak shift to the lower degree. At the same time, this reduction also caused more exposure of the (040) crystal plane at 30.5° and a significant drop in the 29° peak corresponding to the (112) crystal plane. After the load of Co_3O_4 on $BiVO_4$-MoS_2,

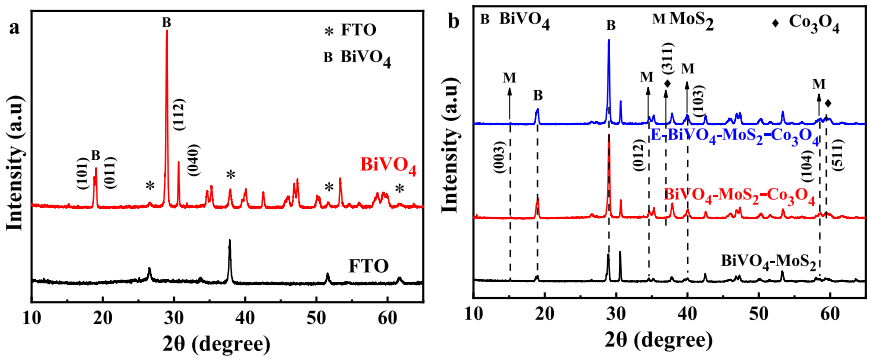

Fig. 2 – X-ray diffraction (XRD) patterns of (a) FTO, $BiVO_4$ and (b) $BiVO_4$-MoS_2, $BiVO_4$-MoS_2-Co_3O_4 and E-$BiVO_4$-MoS_2-Co_3O_4 films.

the peaks shift to the original positions because the film was annealed at 400°C to obtain Co_3O_4 (Zhang et al., 2020).

To further investigate the surface chemical composition and valence state of the samples, XPS studies were performed on the E-$BiVO_4$-MoS_2-Co_3O_4 film electrode and the spectra were given in Fig. 3. XPS survey spectrum in Fig. 3**a** shows that six elements of Bi, V, O, Mo, S, and Co are present in the as-prepared E-$BiVO_4$-MoS_2-Co_3O_4 photoelectrode. Fig. 3**b** shows that the binding energies of Bi $4f_{7/2}$ and Bi $4f_{5/2}$ are 158.8 and 164.1 eV, respectively (Ge, 2008; Chatchai et al., 2009; Ye et al., 2016; Zhao et al., 2018; Hu et al., 2019). Compared with $BiVO_4$-MoS_2-Co_3O_4 (Appendix A **Fig. S5a**), the Bi $4f_{5/2}$ and Bi $4f_{7/2}$ peaks of E-$BiVO_4$-MoS_2-Co_3O_4 show a shift of 0.16 eV to lower binding energy, which indicates that E-$BiVO_4$-MoS_2-Co_3O_4 has more low-valent Bi ions. The binding energies of 516.4 and 523.9 eV of E-$BiVO_4$-MoS_2-Co_3O_4 in Fig. 3**c** were assigned to V $2p_{3/2}$ and V $2p_{1/2}$, which are lower than those of V^{5+}ions in $BiVO_4$ reported in the literature (V $2p_{3/2}$ 517.4 eV and V $2p_{1/2}$ 524.5 eV) (Hu et al., 2018). The peaks of V 2p of E-$BiVO_4$-MoS_2-Co_3O_4 in Appendix A **Fig. S5b** obviously show a shift of 0.08 eV to lower binding energy, indicating that some V^{5+} ions are reduced to V^{4+} after electrochemical modification (Wang et al., 2016, 2017; Hu et al., 2018; Zhao et al., 2018). Figs. 3**b-c** and **S5b** confirmed the existence of sub-stoichiometric $BiVO_4$. Fig. 3**d** shows the results of O 1 s analysis. Three distinct binding energies of 529.5 eV (O_L), 531.5 eV (O_v) and 532.1 eV (O_C) correspond to O^{2-} species in the lattice (O_L) (Sun et al., 2016; Ye et al., 2016), -OH bonded to metal cations in the anoxic zone to maintain charge balance (O_V) (Fan et al., 2016; Wang et al., 2020) and H_2O (Wang et al., 2017), respectively. Compared with the O 1 s of $BiVO_4$-MoS_2-Co_3O_4 in Appendix A **Fig. S5c**, the proportion of O_V in E-$BiVO_4$-MoS_2-Co_3O_4 has increased from 20.34% to 53.54% (Appendix A **Table S1**), which indicates that E-$BiVO_4$-MoS_2-Co_3O_4 has more oxygen vacancies relative to $BiVO_4$-MoS_2-Co_3O_4. The presence of oxygen vacancies can increase the carrier density and improve the charge separation in the film. The binding energies of 231.9 and 235.1 eV in Fig. 3**e** were assigned to the diffraction peaks of Mo $3d_{5/2}$ and Mo $3d_{3/2}$, which are the typical values of Mo^{4+} in MoS_2 (Sun et al., 2016; Ye et al., 2016; Lin et al., 2019; Liu et al., 2020). The diffraction peaks at 780.8 and 796.9 eV in Fig. 3**f** represent Co $2p_{3/2}$ and Co $2p_{1/2}$ (Yan et al., 2010; Shi et al., 2012; Xiang et al., 2013; Hu et al., 2019; Li et al., 2020). The peak of Co $2p_{3/2}$ in E-$BiVO_4$-MoS_2-Co_3O_4 is lower than that in $BiVO_4$-MoS_2-Co_3O_4 (Co $2p_{3/2}$ 781.3 eV shown in Appendix A **Fig. S5d**). This may be due to the presence of oxygen vacancies and the formation of sub-stoichiometric oxides, which is consistent with the previous XPS analysis of Bi 4f, V 2p and O 1 s. The XPS results confirmed that electrochemical treatment can generate oxygen vacancies and cause oxygen species to re-coordinate to produce sub-stoichiometric oxides.

Appendix A **Fig. S6a** shows the UV–Vis spectrum of $BiVO_4$ and E-$BiVO_4$-MoS_2-Co_3O_4 films. It can be seen that the absorbance edge of the photoelectrocatalytic material prepared in this study is about 540 nm. There is almost no absorbance in the light range more than 550 nm. The E-$BiVO_4$-MoS_2-Co_3O_4 film has stronger light absorption than $BiVO_4$, indicating that electrochemical modification and heterojunction composite have a certain promotion effect on light absorption. The bandgap can be estimated by the Kubelka-Munk function according to formula (2):

$$(\alpha h\nu)^{1/n} = A(h\nu - E_g) \quad (2)$$

where α is the absorption coefficient, h (4.136×10^{-15} eV·sec) is the Planck constant, ν is the speed of light 3×10^8 m/sec, c is the constant ($c = 1$), and E_g (eV) is the bandgap energy. The parameter n depends on the characteristics of the transition in a semiconductor, where $n = 1/2$ for direct transitions and $n = 2$ for indirect transitions. As $BiVO_4$ is a direct band gap energy semiconductor (Regmi et al., 2019), the value of $n = 1/2$. As shown in Appendix A **Fig. S6b**, the bandgaps of $BiVO_4$ and E-$BiVO_4$-MoS_2-Co_3O_4 are approximately 2.36 and 2.34 eV, respectively. The results show that the composite catalytic material has a slightly narrower band gap, and can absorb more visible light.

2.2. *PEC performance*

The photocurrent properties of $BiVO_4$, $BiVO_4$-MoS_2, $BiVO_4$-MoS_2-Co_3O_4 and E-$BiVO_4$-MoS_2-Co_3O_4 films were tested by linear sweep voltammetry using 0.1 mol/L NaOH as electrolyte solution. As shown in Fig. 4, the photocurrent density of E-$BiVO_4$-MoS_2-Co_3O_4 film was 6.6 times higher than that of pure $BiVO_4$ at 0.45 V vs. Ag/AgCl under visible light irradiation.

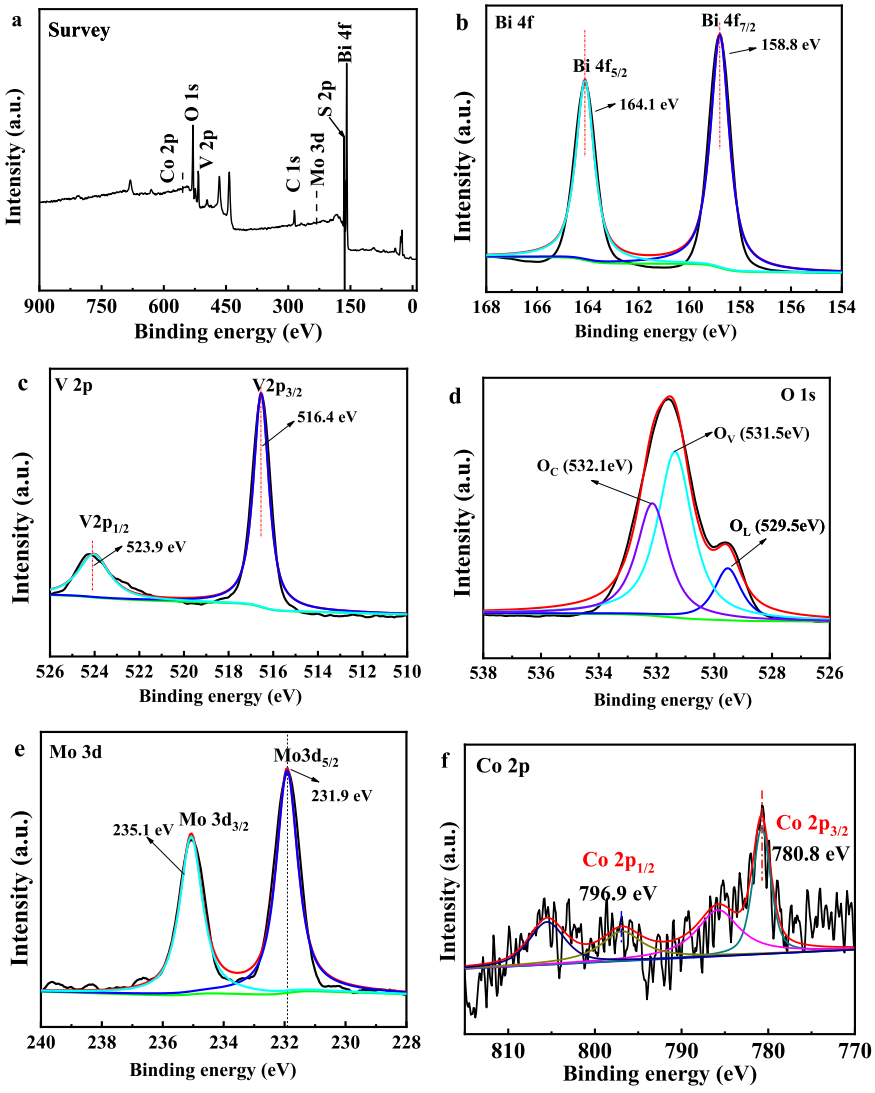

Fig. 3 – X-ray photoelectron spectroscopy (XPS) spectra of E-$BiVO_4$-MoS_2-Co_3O_4 film electrode (a) survey spectrum and high-resolution core spectrum for (b) Bi 4f, (c) V 2p, (d) O 1 s, (e) Mo 3d, and (f) Co 2p.

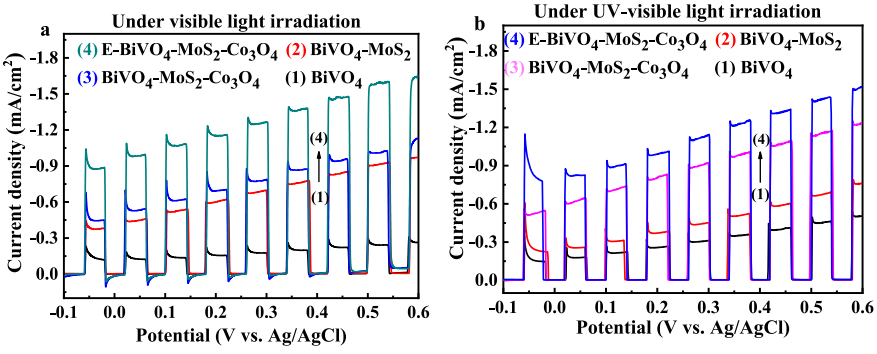

Fig. 4 – Linear sweep voltammetric curves of $BiVO_4$, $BiVO_4$-MoS_2, $BiVO_4$-MoS_2-Co_3O_4 and E-$BiVO_4$-MoS_2-Co_3O_4 films under (a) chopped visible and (b) UV–visible light irradiation in 0.1 mol/L NaOH aqueous solution.

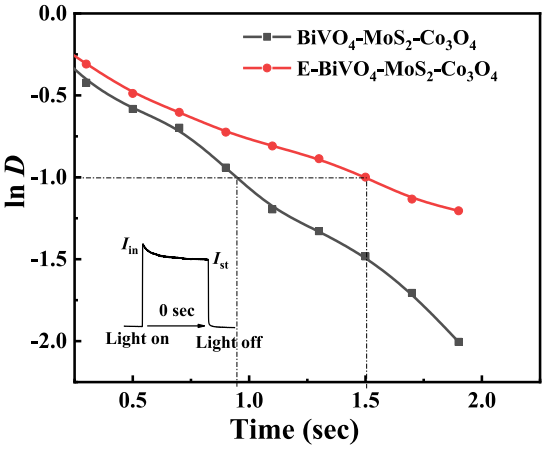

Fig. 5 – Normalized plots of photocurrent as a function of time for different as-prepared films. Inset: typical photocurrent transient response curve at 0.5 V (vs. Ag/AgCl). I_{in}: photocurrent was measured at irradiation time of 0 sec; I_{st}: photocurrent obtained at steady state; D: transient photocurrent.

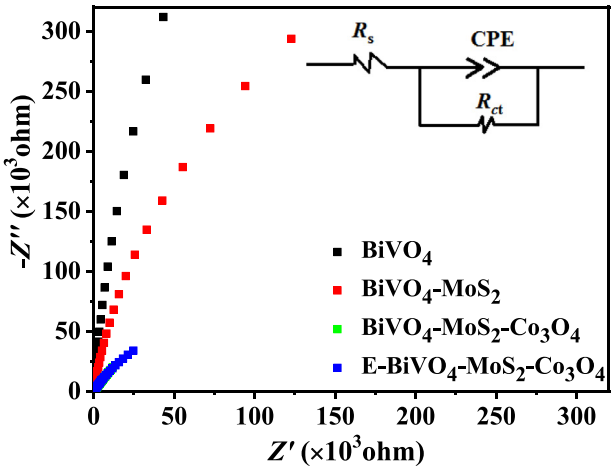

Fig. 6 – Nyquist plots of $BiVO_4$, $BiVO_4$-MoS_2, $BiVO_4$-MoS_2-Co_3O_4 and E-$BiVO_4$-MoS_2-Co_3O_4 films under dark condition in 0.1 mol/L NaOH aqueous solution. The inset shows the equivalent circuit using to fit the Nyquist plots. Z'': imaginary impedance; Z': real impedance; R_s: series resistance; R_{ct}: interface charge transfer resistance; CPE: constant phase angle element.

The influence of electrochemical modification on the PEC performance of $BiVO_4$ can be seen in Appendix A **Fig. S7**. The photocurrents of $BiVO_4$ and $BiVO_4$-Co_3O_4 have been significantly improved after electrochemical modification, which strongly supported that electrochemical modification is an effective approach to increase PEC activity of composite electrodes and sub-stoichiometric $BiVO_4$ formed by electrochemical modification may play an important role (Chen et al., 2011; Wang et al., 2016).

For further determination of charge separation properties, the charge recombination process in the as-prepared film electrodes was compared by testing the transient photocurrent according to formula (3):

$$D = (I_t - I_{st})/(I_{in} - I_{st}) \quad (3)$$

where D represents transient photocurrent, I_{st} (mA/cm^2) is photocurrent obtained at steady state, I_{in} (mA/cm^2) and I_t (mA/cm^2) photocurrent were measured at irradiation time of 0 and t (sec), respectively (Cong et al., 2018).

As shown in Fig. 5, the transient photocurrents of $BiVO_4$-MoS_2-Co_3O_4 and E-$BiVO_4$-MoS_2-Co_3O_4 films were compared at 0.5 V (vs. Ag/AgCl) under visible light irradiation. Among the tested samples, E-$BiVO_4$-MoS_2-Co_3O_4 exhibited the largest t value at the same ln D value. For example, at ln $D = -1$, the t value was estimated to be ca. 1.55 sec for E-$BiVO_4$-MoS_2-Co_3O_4. Whereas, for $BiVO_4$-MoS_2-Co_3O_4 was 0.86 sec. Thus, the slowest recombination rate can be speculated in E-$BiVO_4$-MoS_2-Co_3O_4.

In order to further investigate the charge transfer process of the prepared electrode, the electrochemical impedance spectroscopy (EIS) of $BiVO_4$, $BiVO_4$-MoS_2, $BiVO_4$-MoS_2-Co_3O_4, and E-$BiVO_4$-MoS_2-Co_3O_4 films were measured. Fig. 6 shows that the impedance ring radius of $BiVO_4$-MoS_2-Co_3O_4 and E-$BiVO_4$-MoS_2-Co_3O_4 are smaller. And the impedance ring radius of E-$BiVO_4$-MoS_2-Co_3O_4 is the smallest, which indicates that it has the smallest charge transfer resistance among the as-prepared films. In addition, the equivalent circuit model (inset in Fig. 6) was used to simulate the Nyquist data, where R_s and R_{ct} represent the series resistance and interface charge transfer resistance, respectively. According to Appendix A **Table S2**, compared with the original $BiVO_4$, the R_{ct} values of $BiVO_4$-MoS_2, $BiVO_4$-MoS_2-Co_3O_4 and E-$BiVO_4$-MoS_2-Co_3O_4 electrodes were reduced by 3.3, 9.7 and 18.2 times, respectively, indicating that the composite material greatly enhanced the charge transfer efficiency.

The IPCE of $BiVO_4$, $BiVO_4$-MoS_2, $BiVO_4$-MoS_2-Co_3O_4 and E-$BiVO_4$-MoS_2-Co_3O_4 photoelectrodes at different wavelengths were measured to further investigate the PEC activity of as-prepared films. As shown in Appendix A **Fig. S8**, the IPCE curve trends of the four photoelectrocatalytic films are approximately the same in the absorption range from 400 to 550 nm. The IPCE values of $BiVO_4$-MoS_2, $BiVO_4$-MoS_2-Co_3O_4 and E-$BiVO_4$-MoS_2-Co_3O_4 films at 400 nm were about 16.5%, 26.1%, 28.5%, respectively, which were higher than that of $BiVO_4$ film (2.5%). It further proved that MoS_2, Co_3O_4 and electrochemical treatment can enhance charge separation and improve the PEC activity of $BiVO_4$.

Cyclic voltammetry (CV) analysis was used to calculate the double-layer capacitance of the material, and further evaluated the electrochemical active surface area (ECSA) of the prepared E-$BiVO_4$-MoS_2-Co_3O_4 electrode and $BiVO_4$ electrode through the double-layer capacitance (C_{dl})/specific capacitance (C_s) (Chen et al., 2019; Liu et al., 2019). As shown in Appendix A **Fig. S9**, the electrochemical active area of E-$BiVO_4$-MoS_2-Co_3O_4 (C_{dl} = 0.5195 mF/cm^2) is much larger than that of $BiVO_4$ (C_{dl} = 0.0448 mF/cm^2), which indicates that the prepared E-$BiVO_4$-MoS_2-Co_3O_4 electrode has larger electrochemical active area.

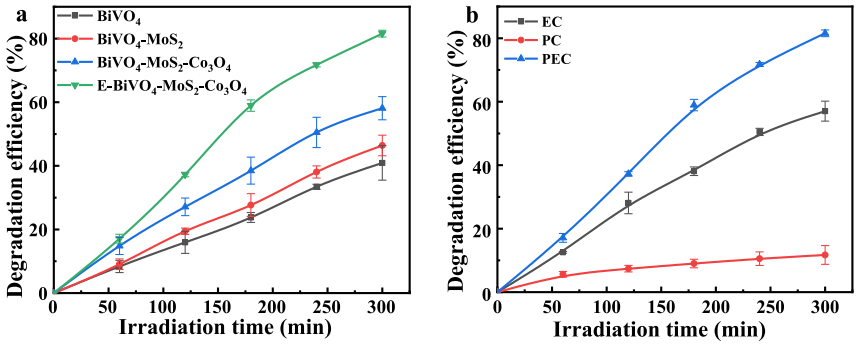

Fig. 7 – (a) Bisphenol A (BPA) degradation by $BiVO_4$, $BiVO_4$-MoS_2, $BiVO_4$-MoS_2-Co_3O_4 and E-$BiVO_4$-MoS_2-Co_3O_4 films in photoelectrocatalysis (PEC); (b) different catalytic processes on BPA degradation over E-$BiVO_4$-MoS_2-Co_3O_4 film. Reaction conditions: 3.5 V, 0.2 mol/L Na_2SO_4, pH ~6.3, 50 mL solution, 10 mg/L BPA. EC: electrocatalysis; PC: photocatalysis.

2.3. *PEC activity for the removal of refractory pollutants*

The removal of contaminants by the prepared E-$BiVO_4$-MoS_2-Co_3O_4 electrode was investigated using BPA as a simulated pollutant. As shown in Fig. 7, E-$BiVO_4$-MoS_2-Co_3O_4 film has better BPA removal efficiency than other PEC films. The degradation process was fitted using a pseudo first-order kinetic model. According to Appendix A **Table S3**, the reaction rate constant of E-$BiVO_4$-MoS_2-Co_3O_4 film is the largest among all electrodes, which is 3.22 times higher than $BiVO_4$. A total organic carbon analyzer (TOC) was used to evaluate the mineralization degree. The TOC removal rate is 61.5% under the optimal condition of BPA removal, which indicates the high mineralization of BPA. The PEC activity of E-$BiVO_4$-MoS_2-Co_3O_4 film for BPA removal was further investigated under PC, EC and PEC conditions. Fig. 7**b** and Appendix A **Table S4** show that the degradation rate of BPA under PC and EC conditions is lower than that of PEC. The reaction rate constant of PEC is 14.5 and 2 times that of PC and EC, respectively, which indicate that the degradation of BPA by E-$BiVO_4$-MoS_2-Co_3O_4 composite film has good efficiency in PEC process. The synergistic effect factor (*f*) was estimated to be about 75.76% for comparative experiments in the degradation process of BPA using the following definition:

$$f = \frac{k_{PEC} - (k_{PC} + k_{EC})}{(k_{PC} + k_{EC})} \times 100\% \quad (4)$$

where k_{PEC}, k_{EC}, and k_{PC} represent the reaction rate constants of BPA degradation under PEC, EC, and PC conditions, respectively.

The degradation intermediates of BPA were investigated by high performance liquid chromatography. Appendix A **Fig. S10a** is a high performance liquid chromatogram of the degradation of bisphenol A by E-$BiVO_4$-MoS_2-Co_3O_4 film. There are four intermediates which are hydroquinone, catechol, phenol, and 4-isopropylphenol in the degradation process of BPA (shown in Appendix A **Fig. S10b**). The intermediates will be further degraded with the reaction going on, and eventually be converted into inorganic substances CO_2 and H_2O.

The stability of E-$BiVO_4$-MoS_2-Co_3O_4 film was investigated by successive cyclic degradation experiments. As shown in Appendix A **Fig. S11**, the degradation rate of BPA remains basically unchanged after five cycles, which indicated that the E-$BiVO_4$-MoS_2-Co_3O_4 composite film has good stability.

2.4. *Proposed mechanism*

In order to investigate the main active species generated in the PEC degradation of BPA by E-$BiVO_4$-MoS_2-Co_3O_4 thin film, several scavengers (*tert*–butanol, oxalic acid, and *p*-benzoquinone) were used in degradation reaction. As shown in Fig. 8**a**, when 10 mmol/L *p*-benzoquinone ($O_2^{\cdot -}$ scavenger) was added, the degradation efficiency of BPA decreased by 29.04%. When 10 mmol/L oxalic acid (h^+ scavenger) was added, the degradation efficiency of BPA decreased by 62.27%. When 10 mmol/L *t*-butanol ($HO^{\cdot}$ scavenger) was added, the removal rate of contaminants remained essentially the same, demonstrating that hydroxyl radicals are not the main active substances to oxidize BPA (Wang et al., 2010). From the above experimental results, it can be inferred that h^+ and $O_2^{\cdot -}$ are the main active species in the PEC degradation of BPA. Electron spin resonance (ESR) was used to further confirm the production of $O_2^{\cdot -}$ during the photocatalytic degradation of BPA. As shown in Appendix A **Fig. S12**, no $O_2^{\bullet -}$ signal is observed in the unexcited state, but there is a strong $O_2^{\cdot -}$ signal after excitation, which means that $O_2^{\cdot -}$ is indeed produced during the degradation of BPA.

On this basis, the mechanism of photocatalytic degradation of BPA by E-$BiVO_4$-MoS_2-Co_3O_4 composite photoelectrocatalytic film was further discussed. As shown in Fig. 8**b**, the conduction bands (CB) of $BiVO_4$ and MoS_2 are at 0.3 and −0.13 V, and the corresponding band gaps are 2.36 and 1.9 eV, respectively (Regmi et al., 2017; Zhang et al., 2017b). Under visible light irradiation ($\lambda > 420$ nm), electrons are excited from the valence band (VB) of $BiVO_4$ or MoS_2 to its corresponding conduction band (CB), forming photo-generated hole-electron pairs. The electrons of MoS_2 can be transferred to the CB of $BiVO_4$, while the holes in the VB of $BiVO_4$ migrate to the VB of MoS_2. Under the external applied potential, the electrons in CB of $BiVO_4$ could be driven to the cathode to reduce oxygen to generate $O_2^{\cdot -}$. Thus, photogenerated electrons and holes were effectively separated. Holes accumulated on the VB of MoS_2 and the surface of Co_3O_4 could oxidize BPA, and finally gen-

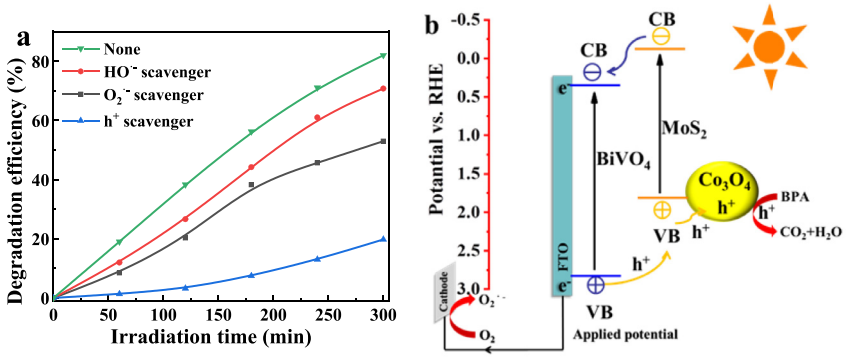

Fig. 8 – (a) Effect of different trapping agents on the degradation of BPA for E-$BiVO_4$-MoS_2-Co_3O_4 film under PEC process; (b) Schematic diagram of the charge transfer process for E-$BiVO_4$-MoS_2-Co_3O_4 under visible light irradiation. h^+: active hole; e^-: active electron; RHE: reversible hydrogen electrode; CB: conduction band; VB: valence band; FTO: fluorine-doped tin oxide substrate.

erate inorganic substances such as CO_2 and H_2O (Appendix A **Fig. S13**). The main reactions in the degradation process of bisphenol A could be expressed as follows:

$$\text{E-BiVO}_4\text{-MoS}_2\text{-Co}_3\text{O}_4 + h\nu \rightarrow \text{E-BiVO}_4\text{-MoS}_2\text{-Co}_3\text{O}_4\ (e^- + h^+) \quad (5)$$

$$e^- + O_2 \leftrightarrow O_2^{\bullet -} \quad (6)$$

$$2e^- + O_2 + 2H^+ \rightarrow H_2O_2 \quad (7)$$

$$H_2O_2 + e^- \rightarrow HO^\cdot + OH^- \quad (8)$$

$$h^+ + OH^- \rightarrow HO^\cdot \quad (9)$$

$$h^+ + \text{bisphenol A} \rightarrow \text{degradation production} \quad (10)$$

$$O_2^{\cdot -} + \text{bisphenol A} \rightarrow \text{degradation production} \quad (11)$$

$$HO^\cdot + \text{bisphenol A} \rightarrow \text{degradation production} \quad (12)$$

The degradation process of bisphenol A mainly includes three stages: (1) the mass transfer of organic compounds from the bulk solution to the electrode surface; (2) the adsorption of organic compounds at the catalytic site of electrode surface; (3) the reaction between the active material and the adsorbed organic molecules. According to the above reaction process and scavenger experiment, it can be seen that the main active substances in the reaction process are h^+ and $O_2^{\cdot -}$. Since the life of h^+ is very short, the reaction related to h^+ mainly occurs on the electrode surface. The active e^- can react with dissolved oxygen in the solution to generate the corresponding active substance ($O_2^{\cdot -}$), which further react with organic compounds in bulk solution (Li et al., 2009). Under the synergetic action of h^+, $O_2^{\cdot -}$ and $HO^\cdot$, BPA was effectively degraded.

3. Conclusions

E-$BiVO_4$-MoS_2-Co_3O_4 thin film electrodes with higher photocatalytic activity were synthesized by hydrothermal method, electrodeposition, and calcination. The photocurrent density of E-$BiVO_4$-MoS_2-Co_3O_4 film under visible light is 6.6 times that of $BiVO_4$ (0.45 V vs. Ag/AgCl). The E-$BiVO_4$-MoS_2-Co_3O_4 thin film electrode can effectively degrade organic pollutants and the degradation efficiency of BPA in PEC process is higher than that in PC or EC process. The reaction rate constant of E-$BiVO_4$-MoS_2-Co_3O_4 film is 3.53 times higher than that of $BiVO_4$. h^+ and $O_2^{\cdot -}$ are the main active species in the PEC degradation of BPA. The enhanced PEC performance benefits from its lower interfacial charge transfer resistance, the formation of oxygen vacancies and sub-stoichiometric metal oxides, and higher separation efficiency of photogenerated electron-hole pairs, which effectively enhance the PEC activity of $BiVO_4$. Moreover, E-$BiVO_4$-MoS_2-Co_3O_4 composite film exhibited good stability.

Acknowledgments

This work was financially supported by the Zhejiang Provincial Natural Science Foundation of China (Nos. LY18B060003, LR18B070001, and LY16B060001), the National Natural Science Foundation of China (Nos. 21576237, 21876154 and 21477114), and Graduate Innovation Foundation of Zhejiang Gongshang University (No. 1260KZN0217059G).

Appendix A. Supplementary data

Supplementary material associated with this article can be found in the online version at doi:10.1016/j.jes.2020.09.027.

REFERENCES

Arora, Y., Shah, A.P., Battu, S., Maliakkal, C.B., Haram, S., Bhattacharya, A., et al., 2016. Nanostructured MoS_2/$BiVO_4$ composites for energy storage applications. Sci. Rep. 6, 36294.

Bao, Q., Hui, K.S., Duh, J.G., 2016. Promoting catalytic ozonation of phenol over graphene through nitrogenation and Co_3O_4 compositing. J. Environ. Sci. 50, 38–48.

Bui, X.T., Vo, T.P.T., Ngo, H.H., Guo, W.S., Nguyen, T.T., 2016. Multicriteria assessment of advanced treatment technologies for micropollutants removal at large-scale applications. Sci. Total Environ. 563-564, 1050–1067.

Chatchai, P., Murakami, Y., Kishioka, S.Y., Nosaka, A.Y., Nosaka, Y., 2009. Efficient photocatalytic activity of water oxidation over WO_3/$BiVO_4$ composite under visible light irradiation. Electrochim. Acta 54, 1147–1152.

Chen, F., Yang, Q., Wang, Y., Zhao, J., Wang, D., Li, X., et al., 2017. Novel ternary heterojunction photcocatalyst of Ag nanoparticles and g-C_3N_4 nanosheets co-modified $BiVO_4$ for wider spectrum visible-light photocatalytic degradation of refractory pollutant. Appl. Catal. B 205, 133–147.

Chen, H., Zhao, Q., Gao, L., Ran, J., Hou, Y., 2019. Water-plasma assisted synthesis of oxygen-enriched Ni-Fe layered double hydroxide nanosheets for efficient oxygen evolution reaction. ACS Sustain. Chem. Eng. 7, 4247–4254.

Chen, L., He, J., Liu, Y., Chen, P., Au, C.T., Yin, S.F., 2016. Recent advances in bismuth-containing photocatalysts with heterojunctions. Chin. J. Catal. 37, 780–791.

Chen, X., Liu, L., Yu, P.Y., Mao, S.S., 2011. Increasing solar absorption for photocatalysis with black hydrogenated titanium dioxide nanocrystals. Science 331, 746–750.

Cong, Y., Ding, W., Zhang, W., Zhang, T., Wang, Q., Zhang, Y., 2020. Fabrication of a novel 3D E-Fe_2O_3-Pi-MoS_2 film with highly enhanced carrier mobility and photoelectrocatalytic activity. Electrochim. Acta 337, 135748.

Cong, Y., Ge, Y., Zhang, T., Wang, Q., Shao, M., Zhang, Y., 2018. Fabrication of Z-Scheme Fe_2O_3–MoS_2–Cu_2O ternary nanofilm with significantly enhanced photoelectrocatalytic performance. Ind. Eng. Chem. Res. 57, 881–890.

Cong, Y., Wang, J., Jin, H., Feng, X., Wang, Q., Ji, Y., et al., 2016. Enhanced photoelectrocatalytic activity of a novel Bi_2O_3-$BiPO_4$ composite electrode for the degradation of refractory pollutants under visible light irradiation. Ind. Eng. Chem. Res. 55, 1221–1228.

Fan, W., Li, H., Zhao, F., Xiao, X., Huang, Y., Ji, H., et al., 2016. Boosting the photocatalytic performance of (001) BiOI: enhancing donor density and separation efficiency of photogenerated electrons and holes. Chem. Commun. 52, 5316–5319.

Fujishima, A., Honda, K., 1972. Electrochemical photolysis of water at a semiconductor electrode. Nature 238, 37–38.

Gauvin, F., Caprai, V., Yu, Q.L., Brouwers, H.J.H., 2018. Effect of the morphology and pore structure of porous building materials on photocatalytic oxidation of air pollutants. Appl. Catal. B 227, 123–131.

Ge, L., 2008. Novel Pd/$BiVO_4$ composite photocatalysts for efficient degradation of methyl orange under visible light irradiation. Mater. Chem. Phys. 107, 465–470.

Giulivo, M., Lopez de Alda, M., Capri, E., Barceló, D., 2016. Human exposure to endocrine disrupting compounds: their role in reproductive systems, metabolic syndrome and breast cancer. A review. Environ. Res. 151, 251–264.

Guo, S., Zhu, Y., Yan, Y., Min, Y., Fan, J., Xu, Q., 2016. Holey structured graphitic carbon nitride thin sheets with edge oxygen doping via photo-Fenton reaction with enhanced photocatalytic activity. Appl. Catal. B 185, 315–321.

Harthcock, C., Qiu, S.R., Mirkarimi, P.B., Negres, R.A., Guss, G., Menor, M.G., et al., 2020. Origin and effect of film sub-stoichiometry on ultraviolet, ns-laser damage resistance of hafnia single layers. Opt. Mater. Express 10, 937–951.

Hu, J., Zhai, C., Zeng, L., Du, Y., Zhu, M., 2018. Enhanced electrocatalytic ethanol oxidation reaction in alkaline media over Pt on a 2D $BiVO_4$-modified electrode under visible light irradiation. Catal. Sci. Technol. 8, 3562–3571.

Hu, L., Zhang, G., Liu, M., Wang, Q., Dong, S., Wang, P., 2019. Application of nickel foam-supported Co_3O_4-Bi_2O_3 as a heterogeneous catalyst for BPA removal by peroxymonosulfate activation. Sci. Total Environ. 647, 352–361.

Huang, H.W., Tu, S.C., Zeng, C., Zhang, T.R., Reshak, A.H., Zhang, Y.H., 2017. Macroscopic polarization enhancement promoting photo- and piezoelectric-induced charge separation and molecular oxygen activation. Angew. Chem. Int. Ed. 56, 11860–11864.

Li, G., Wong, K.H., Zhang, X., Hu, C., Yu, J.C., Chan, R.C.Y., Wong, P.K., 2009. Degradation of acid orange 7 using magnetic AgBr under visible light: the roles of oxidizing species. Chemosphere 76, 1185–1191.

Li, J., Wang, Y., Zhao, S., Jan, A.K., Zhang, X., Zhao, X., 2019. Electrospun nanostructured Co_3O_4/$BiVO_4$ composite films for photoelectrochemical applications. J. Colloid Interface Sci. 539, 442–447.

Li, W., Du, L., Liu, Q., Liu, Y., Li, D., Li, J., 2020. Trimetallic oxyhydroxide modified 3D coral-like $BiVO_4$ photoanode for efficient solar water splitting. Chem. Eng. J. 384.

Lin, J., Wang, P., Wang, H., Li, C., Si, X., Qi, J., et al., 2019. Defect-rich heterogeneous MoS_2/NiS_2 nanosheets electrocatalysts for efficient overall water splitting. Adv. Sci. 6, 1900246.

Liu, T., Li, P., Yao, N., Kong, T., Cheng, G., Chen, S., et al., 2019. Self-Sacrificial template-directed vapor-phase growth of MOF assemblies and surface vulcanization for efficient water splitting. Adv. Mater. 31, e1806672.

Liu, J., Jiang, J., Cheng, C., Li, H., Zhang, J., Gong, H., et al., 2011. Co_3O_4 nanowire@MnO_2 ultrathin nanosheet core/shell arrays: a new class of high-performance pseudocapacitive materials. Adv. Mater. 23, 2076–2081.

Liu, L., Zhao, Q., 2020. A simple fluorescence anisotropy assay for detection of bisphenol a using fluorescently labeled aptamer. J. Environ. Sci. 97, 19–24.

Liu, Y., Sun, J., Lin, S., Xu, Z., Li, L., 2020. In-situ growth of interconnected NiS_2/MoS_2 nanowires supported on Ni foam as binder-free electrode for hybrid supercapacitor. J. Alloys Compd. 820.

Malathi, A., Madhavan, J., Ashokkumar, M., Arunachalam, P., 2018. A review on $BiVO_4$ photocatalyst: activity enhancement methods for solar photocatalytic applications. Appl. Catal. A Gen. 555, 47–74.

Mo, S., He, H., Ren, Q., Li, S., Zhang, W., Fu, M., et al., 2019. Macroporous Ni foam-supported Co_3O_4 nanobrush and nanomace hybrid arrays for high-efficiency CO oxidation. J. Environ. Sci. 75, 136–144.

Pan, Q., Zhang, C., Xiong, Y., Mi, Q., Li, D., Zou, L., et al., 2018. Boosting charge separation and transfer by plasmon-enhanced MoS_2/$BiVO_4$ p–n heterojunction composite for efficient photoelectrochemical water splitting. ACS Sustain. Chem. Eng. 6, 6378–6387.

Regmi, C., Kshetri, Y.K., Kim, T.H., Pandey, R.P., Lee, S.W., 2017. Visible-light-induced Fe-doped $BiVO_4$ photocatalyst for contaminated water treatment. Mol. Catal. 432, 220–231.

Regmi, C., Kshetri, Y.K., Pandey, R.P., Kim, T.H., Gyawali, G., Lee, S.W., 2019. Understanding the multifunctionality in Cu-doped $BiVO_4$ semiconductor photocatalyst. J. Environ. Sci. 75, 84–97.

Shi, P., Su, R., Wan, F., Zhu, M., Li, D., Xu, S., 2012. Co_3O_4 nanocrystals on graphene oxide as a synergistic catalyst for degradation of Orange II in water by advanced oxidation technology based on sulfate radicals. Appl. Catal. B 123, 265–272.

Su, J., Guo, L., Bao, N., Grimes, C.A., 2011. Nanostructured $WO_3/BiVO_4$ heterojunction films for efficient photoelectrochemical water splitting. Nano Lett. 11, 1928–1933.

Sun, M., Wang, Y., Fang, Y., Sun, S., Yu, Z., 2016. Construction of $MoS_2/CdS/TiO_2$ ternary composites with enhanced photocatalytic activity and stability. J. Alloys Compd. 684, 335–341.

Sun, Z., Yu, Z., Liu, Y., Shi, C., Zhu, M., Wang, A., 2019. Construction of 2D/2D $BiVO_4$/g-C_3N_4 nanosheet heterostructures with improved photocatalytic activity. J. Colloid Interface Sci. 533, 251–258.

Wang, C., Zhang, H., Li, F., Zhu, L., 2010. Degradation and mineralization of bisphenol A by mesoporous Bi_2WO_6 under simulated solar light irradiation. Environ. Sci. Technol. 44, 6843–6848.

Wang, D., Li, X., Chen, J., Tao, X., 2012. Enhanced photoelectrocatalytic activity of reduced graphene oxide/TiO_2 composite films for dye degradation. Chem. Eng. J. 198, 547–554.

Wang, G., Yang, Y., Ling, Y., Wang, H., Lu, X., Pu, Y.C., et al., 2016. An electrochemical method to enhance the performance of metal oxides for photoelectrochemical water oxidation. J. Mater. Chem. A 4, 2849–2855.

Wang, J.R., Osterloh, F.E., 2014. Limiting factors for photochemical charge separation in $BiVO_4/Co_3O_4$, a highly active photocatalyst for water oxidation in sunlight. J. Mater. Chem. A 2, 9405–9411.

Wang, S., Chen, P., Yun, J.-H., Hu, Y., Wang, L., 2017. An electrochemically treated $BiVO_4$ photoanode for efficient photoelectrochemical water splitting. Angew. Chem. Int. Ed. 56, 8500–8504.

Wang, S., He, T., Chen, P., Du, A., Ostrikov, K., Huang, W., et al., 2020. In situ formation of oxygen vacancies achieving near-complete charge separation in planar $BiVO_4$ photoanodes. Adv. Mater. 32, 2001385.

Wang, Y., Zheng, Y.Z., Lu, S., Tao, X., Che, Y., Chen, J.F., 2015. Visible-light-responsive TiO_2-coated ZnO:i nanorod array films with enhanced photoelectrochemical and photocatalytic performance. ACS Appl. Mater. Interfaces 7, 6093–6101.

Wu, L., Jin, X., Zhao, T., Wang, H., Dai, Z., 2020. Impact factors of the degradation of bisphenol A by nitrocellulose membrane under illumination. J. Environ. Sci. 100, 193–202.

Xiang, C., Li, M., Zhi, M., Manivannan, A., Wu, N., 2013. A reduced graphene oxide/Co_3O_4 composite for supercapacitor electrode. J. Power Sources 226, 65–70.

Yan, J., Wei, T., Qiao, W., Shao, B., Zhao, Q., Zhang, L., et al., 2010. Rapid microwave-assisted synthesis of graphene nanosheet/Co_3O_4 composite for supercapacitors. Electrochim. Acta 55, 6973–6978.

Ye, L., Jin, X., Ji, X., Liu, C., Su, Y., Xie, H., et al., 2016. Facet-dependent photocatalytic reduction of CO_2 on BiOI nanosheets. Chem. Eng. J. 291, 39–46.

Yu, X.Y., Feng, Y., Jeon, Y., Guan, B., Lou, X.W., Paik, U., 2016. Formation of Ni-Co-MoS_2 nanoboxes with enhanced electrocatalytic activity for hydrogen evolution. Adv. Mater. 28, 9006–9011.

Zhang, S., Wang, L., Liu, C., Luo, J., Crittenden, J., Liu, X., et al., 2017b. Photocatalytic wastewater purification with simultaneous hydrogen production using MoS_2 QD-decorated hierarchical assembly of $ZnIn_2S_4$ on reduced graphene oxide photocatalyst. Water Res. 121, 11–19.

Zhang, T., Zhang, H., Ji, Y., Chi, N., Cong, Y., 2018a. Preparation of a novel Fe_2O_3-MoS_2-CdS ternary composite film and its photoelectrocatalytic performance. Electrochim. Acta 285, 230–240.

Zhang, J., Zhu, Z., Feng, X., 2014. Construction of two-dimensional MoS_2/CdS p-n nanohybrids for highly efficient photocatalytic hydrogen evolution. Chem. Eur. J. 20, 10632–10635.

Zhang, Y., Cui, W.Q., An, W.J., Liu, L., Liang, Y.H., Zhu, Y.F., 2018b. Combination of photoelectrocatalysis and adsorption for removal of bisphenol A over TiO_2-graphene hydrogel with 3D network structure. Appl. Catal. B 221, 36–46.

Zhang, H., Ding, H., Wang, X., Zeng, C., Lu, A., Li, Y., et al., 2017a. Photoelectrochemical performance of birnessite films and photoelectrocatalytic activity toward oxidation of phenol. J. Environ. Sci. 52, 259–267.

Zhang, S., Pu, W., Chen, A., Xu, Y., Wang, Y., Yang, C., et al., 2020. Oxygen vacancies enhanced photocatalytic activity towards VOCs oxidation over Pt deposited Bi_2WO_6 under visible light. J. Hazard. Mater. 384, 121478.

Zhao, X., Lu, Z., Ma, W., Zhang, M., Ji, R., Yi, C., et al., 2018. One-step fabrication of carbon decorated $Co_3O_4/BiVO_4$ p-n heterostructure for enhanced visible-light photocatalytic properties. Chem. Phys. Lett. 706, 440–447.

Zhu, M., Sun, Z., Fujitsuka, M., Majima, T., 2018. Z-scheme photocatalytic water splitting on a 2D heterostructure of black phosphorus/bismuth vanadate using visible light. Angew. Chem. Int. Ed. 57, 2160–2164.

Zia, J., Ajeer, M., Riaz, U., 2019. Visible-light driven photocatalytic degradation of bisphenol-A using ultrasonically synthesized polypyrrole/K-birnessite nanohybrids: experimental and DFT studies. J. Environ. Sci. 79, 161–173.